Signatures of nontopological patches on the surface of topological insulators

Tamoghna Barik [1] and Jay D. Sau [2]

[1] *Condensed Matter Theory Center, Department of Physics, University of Maryland, College Park, Maryland 20742, USA*

[2] *Condensed Matter Theory Center, Department of Physics and Joint Quantum Institute, University of Maryland, College Park, Maryland 20742, USA*

(Received 23 September 2021; revised 22 December 2021; accepted 12 January 2022; published 20 January 2022)

The nontrivial topology in the layered $FeTe_{0.55}Se_{0.45}$ superconductor has been suggested by both theory and experiment to be strongly dependent on the Te concentration. Motivated by this together with the Te fluctuations expected from alloy disorder, we develop a simple layered model for a strong topological insulator that allows us to describe a scenario where topologically trivial domains permeate the sample. We refer to such a phase as topological domain disordered and study the local density (LDOS) of the topological surface states that can be measured using scanning tunneling spectroscopy (STS) in this phase. We find that topologically trivial domains on the surface, where one would expect the topological surface state to be absent, appear as regions of suppressed LDOS surrounded by domain walls with enhanced LDOS. Furthermore, we show that studying the energy dependence of the STS should allow us to distinguish the topologically trivial parts of the surface from other forms of disorder. Finally, we discuss implications of such local disappearance of the topological surface states for the observation of Majorana modes in vortices.

DOI: 10.1103/PhysRevB.105.035128

I. INTRODUCTION

Recently an iron based chalcogenide superconductor, $FeTe_{.55}Se_{.45}$ (FTS), has been found to host a strong topological insulator (TI) phase which is both predicted by first principle calculations [1,2] and later confirmed in the experiments [3,4]. Angle resolved photoemission spectroscopy (ARPES) measurements on this FTS system have shown evidence of parity inversion at the $Z(0, 0, \pi)$ point [3] along with the existence of single Dirac dispersion spectrum at the surface [3–5]. The coexistence of superconductivity and the TI phase in the same material leads to an exciting possibility of realizing Majorana bound states (MBSs) in vortex cores [6–10]. Such MBSs are of particular interest as the building blocks for fault tolerant quantum computing [11–13]. Interestingly, evidence for such MBSs in the form of zero bias peaks (ZBPs) within the vortex cores have been observed using scanning tunneling spectroscopy (STS) by several independent groups [14–16]. The FTS superconductors also appear to be low density (Fermi energy) superconductors relative to the superconducting gap in this system. This allows one, in principle, to separate the MBS from Caroli–de Gennes–Matricon (CdGM) states [14,17] that generically exist in superconducting vortices [18,19]. Perhaps, one of the most encouraging signatures of MBSs is the observation of nearly quantized conductance into vortex cores [20], which is one of the most unique aspects of MBS.

However, the ZBPs are not present in all the vortices [14,16] and the conductance plateau for most of the ZBPs are significantly less than unity [20]. The reduction of the percentage of ZBPs within vortices with increasing magnetic field seen in [14,16] has been argued to arise due to increased coupling between nearby MBSs with decreasing intervortex distances in a recent theoretical work [21]. Another proposed explanation for the disappearance of ZBPs is the delocalization of the MBSs due to the interplay of impurity induced Zeeman field and spin-orbit coupling [22]. While the former explanation will be relatively benign to MBSs at low density, the latter mechanism would be associated with quasiparticle poisoning that would be detrimental to a Majorana qubit. Such quasiparticle poisoning is consistent with the suppression of the conductance height for most of the ZBPs seen in recent experiments [20]. Furthermore, magnetic field induced alignment of Fe impurity magnetic moments has been shown to give rise to the half quantum anomalous Hall phase locally where the vortices would lack any MBSs [23]. However, a more complete understanding of disorder that can affect the details of vortex MBSs is still lacking in the literature. One example that we focus on in this work is the role of Te/Se composition fluctuations on the topological surface states that MBSs rely on.

The importance of the Se/Te concentration fluctuations becomes obvious on considering the fact that Te doping is necessary to drive topologically trivial FeSe into a nontrivial phase, $FeTe_{1-x}Se_x$ (FTS) at $x = 0.45$. The dependence of the topological character in FTS systems on x is further supported by first principle calculation [1], which finds that increasing Te concentration, $(1 - x)$, shifts the center of the p-type band to lower energies facilitating band inversion. This sensitivity of the topological nature of FTS to Te doping is consistent with recent ARPES experiments [24], where the topological surface states are found to disappear below a certain Te doping. Since in $FeTe_{.55}Se_{.45}$ the topological phase appears to occur in the alloy phase, fluctuations in x are likely to occur in much of the sample. This can lead to local variations of the topological invariant on the surface in which case the topological surface states may disappear from parts of the surface. As

we will discuss in the next section, we expect small fluctuations in x to be able to drive such variations in the topological invariant. We will refer to this phase as a topological domain disordered phase. As we will discuss in Sec. IV, such local fluctuations that lead to the local disappearance of the surface state from the top layer of the sample are expected to affect the properties of MBSs in the system as probed by STS.

While variation of parameters in the Hamiltonian of any strong TI can lead, in principle, to the fluctuation of a local topological invariant [25,26], the layered nature of FTS provides a system where the topological invariant can vary on the scale of a single atomic plane. This, potentially, allows access to such domain wall physics using STS. From a theoretical standpoint, this layered nature allows us to construct a relatively simple phenomenological model of the topological phase by considering nearest neighbor tunneling between the layers of electrons. The phenomenological model is determined almost entirely by the symmetries (i.e., properties under C_4 rotation) of the low-energy bands near zero momentum and is independent of the complex details of the strongly correlated spectrum of a layered material. In this work, we choose parameters so that the bulk bands and the computed surface state dispersion match the surface spectrum measured in ARPES [3,4] within the relevant energy and momentum scale (Sec. III A). We then use this model to study the effect of a disorder potential in the band-inversion parameter on the LDOS within the energy window of Dirac dispersion (Sec. III B). This disorder potential realizes the topological domain disordered phase. Finally, we contrast the variation of surface LDOS to the more conventional case of chemical potential disorder to provide a signature of the topological domain disordered phase that is detectable in experiment (Sec. III C).

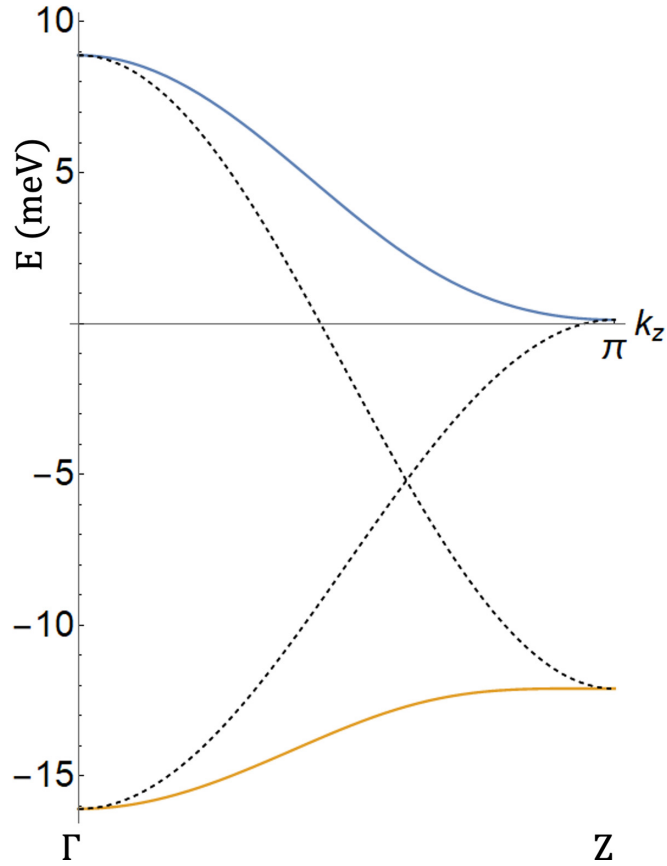

FIG. 1. ΓZ band dispersion from our model $\hat{H}_I$, for the parameter values described in the text, without SOC (dashed curve), i.e., $t' = 0$ in our model, and with SOC (solid curve) are shown. Crossing between d-type and p-type bands happens for $|\delta_\parallel| < |\delta_z|$ (dashed). Hybridization between them via SOC opens up a gap (solid).

II. EFFECTIVE MODEL

A. Motivation

In order to gain insight required to develop an effective model for the topological surface states of FTS, let us consider the dispersion for the FTS system along the ΓZ line (Fig. 1), which shows a band inversion between the even parity d_{xy} band and the odd parity p_z band [1]. This band inversion, absent in FeSe (i.e., for $x = 1$), along with a spin-orbit coupling (SOC) induced insulating gap is responsible for the topological surface states. The top of the valence band at the Z point has inverted parity like p band in Fig. 1 and it is seen to be only about 20 meV below the Fermi energy as found in experiments [3]. This value is significantly smaller when compared to first-principle calculations [1], where the valence band is found to be about 0.5 eV below the Fermi energy at Z. Assuming that the large shift $\sim$1.5 eV of the p band with Te concentration changing from $(1 - x) = 0$ to $(1 - x) = 0.5$, as found in first principles calculations [1], is qualitatively consistent with the real material and the flat d band comparatively remains close to the Fermi energy for both the cases, one would expect the composition $x = 0.45$ to be precariously close to the topological phase boundary by only about $\delta E \sim 0.5 \times 0.02/1.5$ eV ~ 5 meV.

The fact that the composition of $FeTe_{.55}Se_{.45}$ is near the topological phase boundary appears to be consistent with a recent spatially resolved ARPES experiment [24]. Spatially resolved electron diffraction spectroscopy (EDS) analysis of a large sample revealed significant fluctuations in the Fe/Te/Se density distribution over various length scales. This is consistent with the atomic scale topographic image of the surface of $FeTe_{.55}Se_{.45}$ [27], which shows spatial inhomogeneity in Te density profile on the surface. The ARPES experiment in [24] correlated the spatially resolved ARPES data to EDS data to estimate the composition dependence of the topological phase. Using this analysis, the experiment [24] has found that $FeTe_{.55}Se_{.45}$, though topological, resides close to the phase boundary between the topological and trivial phases since small variations of the Te concentration are seen to destroy the topological surface states.

B. Model Hamiltonian

We construct an effective model for the strong TI phase including a pair of bands with opposite parity (d type and p type). We label the even (d-type) and odd (p-type) parity bands by $\rho_z = \pm 1$, respectively. Adding the $j_z = \pm 1/2$ angular momentum degree of freedom described by the set of Pauli matrices $\sigma_{\alpha=x,y,z}$ leads to a model similar to the Bernevig-Hughes-Zhang (BHZ) model for each layer [28] as elaborated below. Our model for FTS respects inversion

symmetry, described by the operator ρ_z, and time reversal symmetry (TRS), described by the operator $i\sigma^y K$. Here K is the complex conjugation operator. The fourfold rotational symmetry around the z axis (C_4) for FTS results in an effective rotational symmetry at long wavelengths. The p_z-type band that we consider is invariant under C_4 rotation and has orbital angular momentum $l_z = 0$ and hence total angular momentum $j_z = \pm 1/2$ including spin. In contrast, the $d_{xz} \pm id_{yz}$ bands have orbital angular momenta $l_z = \pm 1$. A large spin-orbit splitting between them gives rise to a pair of d bands with total angular momenta $j = l + s = 3/2, 1/2$. Thus, combining the two orbital sectors (p_z and $d_{xz} \pm id_{yz}$), we obtain two sectors with total angular momentum $j_z = \pm 1/2$ (one of d_{xy} type and one p_z type) but with opposite parity. By applying the appropriate unitary transformation, we can define $\sigma_z = 2j_z$ in this manifold. This implies the C_4 rotation operator to be $C_4 = e^{i\pi j_z/2} = e^{i\pi\sigma^z/4}$. In the more rigorous group theory representation (e.g., in the DFT based calculation [1]), the states $\rho_z = \pm 1$ correspond to states in the $\Gamma_6^{\pm}$ representations at the Γ and Z points. Focusing near small in-plane momenta (i.e., $k_x, k_y \simeq 0$), the Hamiltonian in this space of $\Gamma_6^{\pm}$ states, under the symmetry constraints and the approximation of nearest neighbor tight binding along the z direction, can be written as

$$\hat{H}_I(k_\parallel \simeq 0, k_z) = \left[\delta_\parallel + \delta_z \cos k_z - \frac{A}{2}\left(k_x^2 + k_y^2\right)\right] \times \sigma^0\rho^z + t' \sin k_z \sigma^z \rho^x, \quad (1)$$

where $\rho_z = \pm 1$ correspond to $\Gamma_6^{\pm}$ states, being the two sectors of odd (even) parity, and $\sigma_z = \pm 1$ correspond to the two angular momentum sector of $j_z = \pm 1/2$ as described above. Here the parameters $\delta_{\parallel,z}$ determine the energy differences between the $\Gamma_6^{\pm}$ states at the Γ and Z point, which are written as $\delta_\parallel + \delta_z$ and $\delta_\parallel - \delta_z$, respectively. Thus, if $|\delta_z| > |\delta_\parallel|$, the two bands can cross somewhere along the ΓZ line facilitating band inversion as seen in Fig. 1, which is plotted for $\delta_z = -9.3$ meV, $\delta_\parallel = -3$ meV, and $t' = 7.5$ meV. In our model [Eq. (1)] it corresponds to the coefficient of ρ^z changing sign while going from Γ to Z, which implies the valence band states have opposite parity eigenvalues at these two time reversal invariant momenta (TRIMs). This is the condition for a band inversion to occur which leads to a nontrivial strong TI phase [29]. The second term describes an SOC which hybridizes the two d and p type $\rho_z = \pm 1$ sectors to open up a gap along the ΓZ ($k_z : 0 \to \pi$) direction (Fig. 1), which is required for the system to have an insulating gap. Note that, while FTS is a superconducting material, a topological surface state in a range of in-plane momentum $k_{x,y}$ can only exist in a range of energy where there is a gap as the perpendicular momentum, k_z, changes. This does not preclude a superconducting state from gapless states at different in-plane momenta from the topological surface states. The flatness of the valence band along ΓZ (band width of $\leqslant 4$ meV as in [3]) justifies the tight binding approach used to model the dispersion along k_z direction. The parameter A in the first term of $\hat{H}_I(k_\parallel \simeq 0, k_z)$ determines the curvature of the parabolic dispersion for small in-plane momenta ($k_\parallel \simeq 0$) around the Γ point. A system with the Hamiltonian Eq. (1) with $\delta_{\parallel,z}$ chosen to be in the topological regime ($|\delta_z| > |\delta_\parallel|$) hosts topological surface states on the (001) surface with in-plane Dirac dispersion. The corresponding velocity for the dispersion near the Γ point is determined by a SOC term given by

$$\hat{H}_{SOC} = \alpha(k_x\sigma^x + k_y\sigma^y)\rho^x. \quad (2)$$

Finally, since the ARPES spectrum of the FTS system does not appear to show particle-hole symmetry [3,4], we include the corresponding symmetry breaking term as follows:

$$\hat{H}_{eh} = \delta_2 \cos k_z \sigma^0 \rho^0. \quad (3)$$

The three terms described above can be combined to obtain our model Hamiltonian

$$\hat{H} = \hat{H}_I + \hat{H}_{SOC} + \hat{H}_{eh}, \quad (4)$$

which can describe the surface states of FTS in the topological phase along with a bulk spectrum that is consistent with ARPES measurements of the (001) surface for parameters described later.

III. NUMERICAL RESULTS FOR SURFACE STATE SPECTRA

A. Ideal surface state

For the purpose of simulating states localized at the (001) surface, it is necessary to represent the Hamiltonian in Eq. (4) in real space along the z direction. We do this by discretizing the z direction with a lattice parameter c. The resultant Fourier transform translates $\cos k_z$ to $\cos k_z \to (|z\rangle\langle z + c| + \text{H.c.})/2$ and $\sin k_z$ by $\sin k_z \to i(|z\rangle\langle z + c| - \text{H.c.})/2$. Here z is the real-space coordinate representing planes stacked in the z direction. Using the resulting discretized Hamiltonian we simulate the surface states for each (k_x, k_y) around the Γ point numerically.

The calculated surface dispersion and the bulk bands near the Γ point are shown in Fig. 2. The energy dispersion curve (EDC) for the broad parabolic bulk band has been shown by the blue line and that of the Dirac dispersion by the red line. The parameters in Eqs. (1)–(3) are tuned to be $\delta_z = -9.3$ meV, $\delta_\parallel = -3$ meV, $t' = 7.5$ meV, $\delta_2 = 1.2$ meV, $A = 798$ meV Å^2, and $\alpha = 266$ meV Å, such that the relevant quantities from the simulated dispersion match the estimates from the ARPES measurements in [3,4], viz. (i) the band width of the valence band along ΓZ direction in Fig. 1 (about 4 meV [3]), (ii) the energy gap between the Dirac point and the top of the bulk valence band ($\sim$10 meV), and (iii) the Dirac velocity for the surface states dispersion ($\sim$370 meV Å), the latter two of which are measured in Refs. [3,4]. In Refs. [3,5], there are similar dispersions for the surface states from a phenomenological model like ours but with important differences in the quantities listed above.

B. Disordered surface state

We now use the parameters determined in the previous paragraph to study tunneling properties of the topological domain disordered phase. As discussed in the Introduction, such a phase can arise from local fluctuations in the Se concentration, x. We model these fluctuations by allowing the parameter $\delta_\parallel$ in the Hamiltonian [Eq. (1)] to vary in space (x-y-z) according to the relation $\delta_\parallel(x, y, z) = \delta_\parallel + w(x, y, z)$,

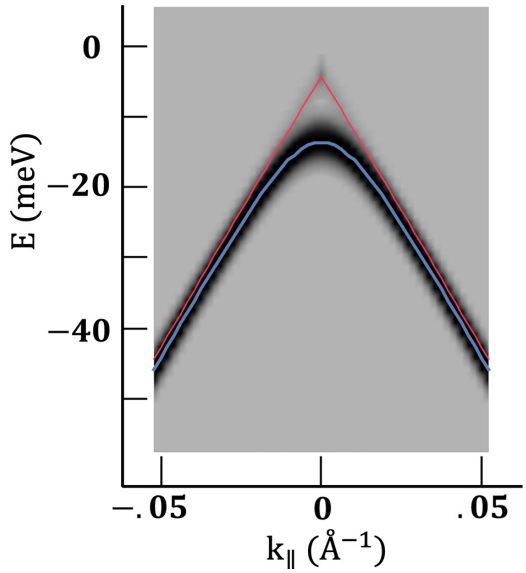

FIG. 2. Surface-weighted parabolic bulk dispersion and the Dirac dispersion for the surface states along with their energy dispersion curves (EDC) shown in blue and red, respectively, as obtained from our model with the parameters specified in the text.

where $w(x, y, z)$ is random with a Gaussian distribution. Motivated by the layered structure of FTS, we assume $w(x, y, z)$ to be smooth in each x-y plane, but uncorrelated between neighboring layers. For the purpose of conceptual and also computational simplicity, we start by assuming that $w(x, y, z)$ varies along the x and z direction but is uniform along the y direction, i.e., $w(x, y, z) \equiv w_{1D}(x, z)$. As mentioned earlier, we assume that the disorder fluctuations are uncorrelated between different layers along z. However, motivated by the strong in-plane electronic dispersion [4] as well as correlation between the positions of Se atoms in the plane [14,27], we assume that $w_{1D}(x, z)$ has a finite correlation length along the x direction that is represented by its Fourier transform along x having the form

$$w_{1D}(k_x, z) = \frac{\sigma_w}{\sqrt{2}} \exp\left[-\frac{(k_x\lambda)^2}{2}\right][X + iY]. \tag{5}$$

In the above, X and Y are two random variables for each value of k_x, z, which are chosen from the normal distribution, $N(0, 1)$. σ_w and λ are respectively the amplitude and characteristic length scale of the disorder potential. We estimate the typical length scale of Te density variation to be 3 nm from STS topographic images from the experiments [27] and use that as the value for λ. Since the potential $w_{1D}(x, z)$ breaks translation invariance along x, it is necessary to replace the k_x momentum in Eq. (1) by $k_x \to -i\partial_x$, where ∂_x is a discretized derivative with an in-plane lattice parameter a.

The numerical results for the surface density of states in the case where $\delta_\parallel(x, y, z)$ varies along the x and z directions, which is calculated using the approach described in the previous paragraph, are shown in Fig. 3. Here Fig. 3(a) shows the profile of $\delta_\parallel(x)$ on the top layer, i.e., $z = 0$. As discussed in Sec. II B, regions with $|\delta_\parallel| < |\delta_z|$ are in a nominally trivial phase, while the rest of the surface is in the topological phase. To help identify trivial regions, Fig. 3(a) plots $\delta(x) = |\delta_\parallel(x)|/|\delta_z| - 1$, so that trivial domains on the otherwise topological surface would appear as regions with $\delta(x) > 0$. As discussed in the Introduction, this local attribution of trivial and topological is more as a guide to understanding the numerical results that follow rather than a strict identification (since a topological phase is strictly speaking a global property). The LDOS associated with this disorder realization applied to the Hamiltonian Eq. (4) is plotted for the top (i.e., $z = 0$) and the second layer (i.e., $z = c$) of the system in Fig. 3(b). We notice that the top layer LDOS is suppressed at the nominally trivial regions, whereas the second layer LDOS is enhanced. The same observation holds for different energies within the Dirac dispersion window. In fact, the normalized LDOS for the top layer at different energies nearly collapse on each other as shown in Fig. 3(c) if scaled appropriately. This suggests that the conclusion that the Dirac surface states are transferred from the top layer to the layer below in the locally

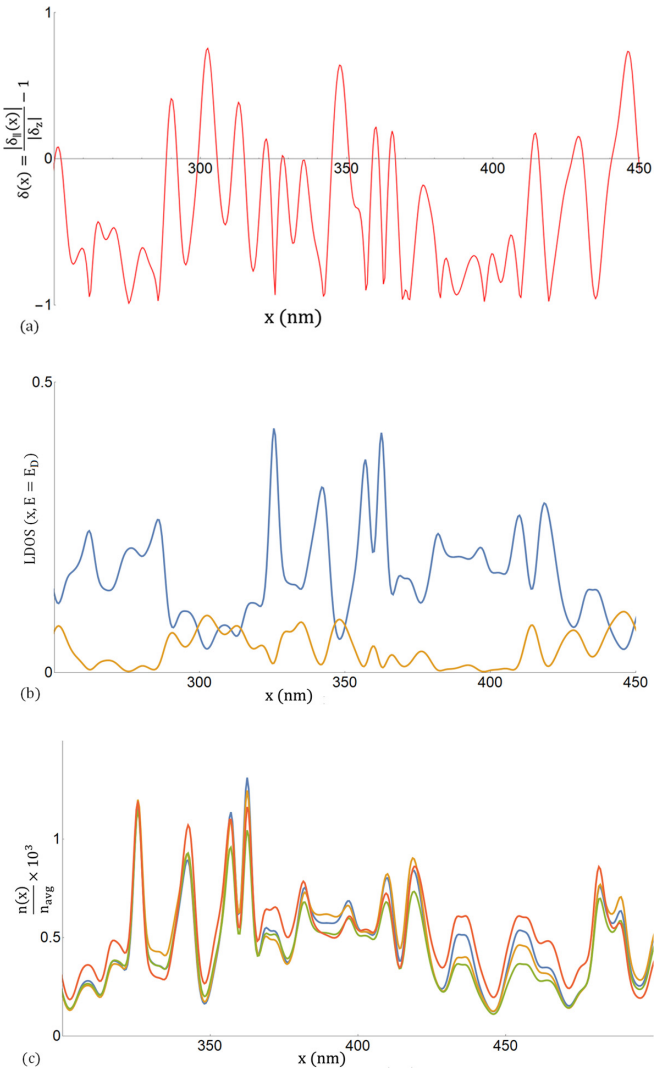

FIG. 3. (a) $|\delta_\parallel(x)|/|\delta_z| - 1$ plotted as the red curve where the black lines show some of the topological $[\delta(x) < 0]$ and trivial $[\delta(x) > 0]$ phase boundaries. (b) Top layer (blue) and second layer (yellow) LDOS for the topological domain disorder. (c) Normalized top layer LDOS at different energies within the Dirac dispersion window collapse on each other.

trivial region applies over a range of energy. This transfer of LDOS between the layers would be difficult to measure in STS. However, a closer examination of Fig. 3(b) shows that the trivial regions represented by LDOS enhancement in the second layer occur in the vicinity of large LDOS peaks in the top layer near the topological-trivial boundaries. Such peaks in the LDOS on the top layer that demarcate the trivial domains may be visible in STS.

The more obvious signature of a trivial patch on the surface of a strong topological insulator would be the reduced local density of states seen in Fig. 3(b). However, as also apparent from this plot, dips in local density of states are also seen in areas of strong fluctuations of $\delta(x)$, which are otherwise topological. This is consistent with the fact that disorder-induced Fermi energy fluctuations on the surface can lead to the Dirac point crossing the local Fermi level. The local density of states would be expected to be suppressed at such a point, since the density of states of the Dirac dispersion in two dimensions vanishes at the Dirac point.

C. Topological domain disorder versus chemical potential disorder

To determine distinctive features associated with topological domain disorder relative to conventional charge density fluctuations, we simulate the LDOS in the presence of chemical potential disorder with a Gaussian distribution. For this purpose, we keep $\delta_\parallel$ fixed and add a Gaussian disorder potential proportional to the identity matrix, $w(x)\sigma^0\,\rho^0$, to the Hamiltonian in Eq. (4). We choose the amplitude of chemical potential fluctuations to be about 2 meV (estimated from the broadening of the Dirac point in ARPES measurement [3,4]) and choose the same length scale ($\lambda \simeq 3$ nm) for the disorder variation similar to Eq. (5). Looking at the normalized top layer LDOS plot at several energies [Fig. 4(a)], we notice that, unlike the case of topological domain disorder, the LDOS profiles at various energies are distinct in shape and do not collapse on each other upon scaling in stark contrast to the case of topological domain disorder. The difference of the profiles in this case for different energies is related to the dependence of the length scale for LDOS variation, ξ, with energy as $\xi(E) \propto 1/(E - E_D)$ around the Dirac energy E_D [Fig. 4(b)].

Hence the LDOS variation within the Dirac dispersion window is distinct between the cases of topological domain disorder and chemical potential disorder. The two cases can be distinguished by comparing the normalized LDOS at various energies and the energy dependence of the characteristic length scale for LDOS variation, $\xi(E)$, for the top layer. Thus the LDOS peaks in Fig. 3(b) that are in the vicinity of a topologically trivial patch can potentially be distinguished from peaks associated with chemical potential fluctuations based on their energy independence. Besides the energy independent peaks, another signature of the LDOS features associated with topological domain disorder is the energy independence of the characteristic length scale. We estimate the characteristic length scale ξ for the LDOS variation as the inverse of the width, Δk_x, of the Fourier spectrum of the LDOS (i.e., quasiparticle interference spectrum) according to the relation $\xi \simeq 1/\sqrt{\langle \Delta k_x^2 \rangle}$. Figure 4(b) shows a plot of the length scale

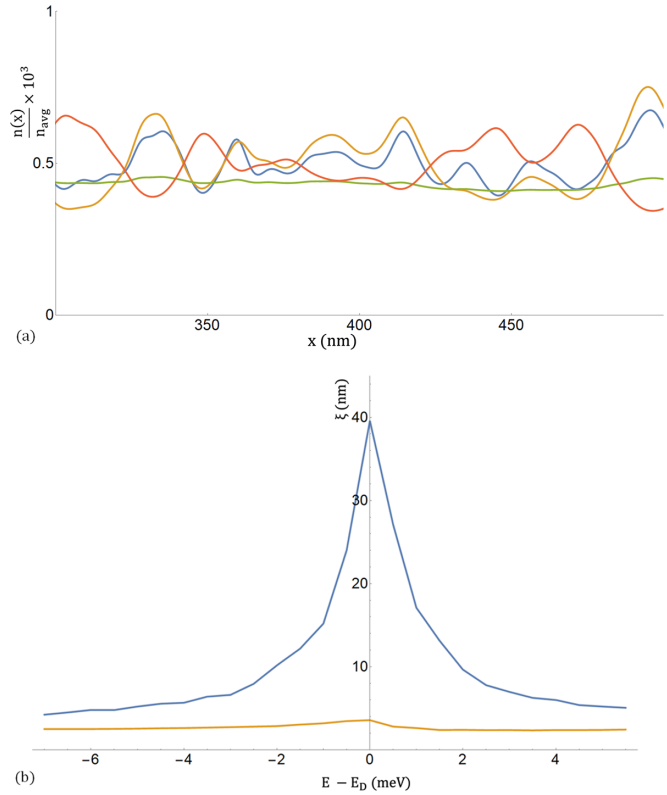

FIG. 4. (a) Normalized LDOS at different energies for the chemical potential disorder. (b) Comparison of energy dependence of LDOS-LDOS correlation length between the topological domain disorder (orange) and the chemical potential disorder (blue) cases.

ξ as a function of the tunneling energy relative to the Dirac point. We find that for chemical potential disorder (shown in blue) ξ increases substantially as energy is reduced. This is in contrast to topological domain disorder (shown in yellow) where the associated length scale ξ is seen to be energy independent in Fig. 4(b). This conclusion is consistent with the collapse of the various LDOS peaks seen in Fig. 3(c), which shows that the widths of peaks at the edge of trivial regions are independent of energy. This can be understood as these peaks being associated with tunneling into domain walls, whose widths are controlled by spatial variation of the disorder parameter $\delta(x)$.

The results discussed so far have been based on a simplified model for disorder where the variation of the disorder parameter along the y direction was ignored. Finally, we present the results from the simulation of a more realistic model where the topological domain disorder is introduced in 2D at each layer. The corresponding disorder potential in momentum space for each layer, $w_{2D}(k_x, k_y, z)$, can be obtained by substituting k_x in Eq. (5) by $k_\parallel = \sqrt{k_x^2 + k_y^2}$. In this case the trivial islands [shown as white regions on the top layer in Fig. 5(a)] are finite in size along all directions. The 2D LDOS is plotted using a color plot in Fig. 5(b) for the top layer and the next layer in the upper panel and lower panel, respectively. Correlating to the trivial island picture in Fig. 5(a) it can be noted that at the trivial regions the top layer LDOS is reduced, whereas the second layer LDOS is increased, consistent with the result

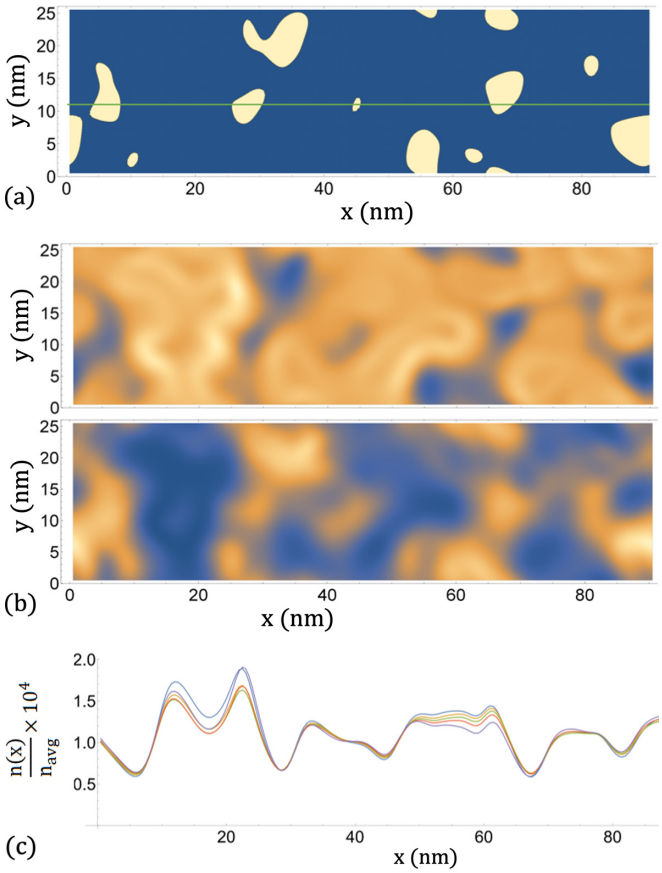

FIG. 5. (a) Trivial islands shown as white patches, whereas the dark blue region is topological; (b) top layer 2D LDOS and next layer 2D LDOS shown in color map in the upper and lower panel, respectively, where the density gradient goes high to low from yellow to dark blue. (c) Normalized top layer LDOS plot at five different energy values along the green line marked in (a).

for the 1D disorder case as discussed before. Moreover, the energy collapse feature of the LDOS at different energies [as shown for a section of the sample on the top layer in Fig. 5(c)] is also present in the 2D disordered case.

In our model the suppression of the LDOS on the trivial regions of the top layer and the correlated enhancement of the same on the next layer can be explained as follows. The topologically trivial domains on the top layer do not let any of the Dirac surface states penetrate inside them. Rather, the layer below the top layer at those regions provides the boundary between the bulk topological phase and the trivial phase residing on the top layer, which implies that the gapless states are shifted below to the next-to-top layer that is topological.

IV. SUMMARY AND DISCUSSION

In this work, we have studied the effect of alloy disorder (i.e., Te/Se composition fluctuations) on the topological surface state of FTS. In order to do this, we have introduced a variant of the BHZ model [28] for the strong TI phase that is appropriate to a layered system such as FTS where the bandwidth from out-of-plane tunneling is much smaller than the in-plane bandwidths. Similar to the BHZ model, the topological properties such as the surface state dispersion and the near-gap bulk band structure can be characterized with a few phenomenologically determined parameters. We have fit our model to ARPES [3,4] and been able to reproduce the qualitative structure of the surface ARPES dispersion. The BHZ model, which is based on a small wave-vector approximation, is not appropriate to FTS because of the narrow band width in the out of plane direction. Our phenomenological model can be combined with input from DFT calculations [1] to model the effect of Te composition fluctuations as a shift of the odd parity p_z band. As a side note, our phenomenological approach to model topological invariant fluctuations can be modified for the 2D FTS system which also possesses nontrivial topological properties as a function of x [30]. We find that fluctuations in the position of the odd parity band can drive local fluctuations in the topological invariant, which in turn can lead to the disappearance of the surface state in parts of the surface for the 3D sample. More generally the fluctuations in topological invariant can also be driven by the change of the interlayer hopping term, denoted by δ_z in our model as the invariant is determined by the ratio of the on-site potential difference, $\delta_\parallel$, and interlayer hopping amplitude, δ_z, denoted by $\delta(x) = |\delta_\parallel(x)/\delta_z|$. Since the interlayer hopping amplitude is mediated by the atomic orbitals from the next-to-top layer, the composition of Se/Te only on the topmost layer may not correlate to the local topological property on the surface of the sample. The disappearance of the surface state at the trivial domains is marked by a reduced local density of states on the top surface in these areas, which are bounded by domain walls of peaks in the LDOS. One complication that we discuss is that the suppressed density of states in the nontopological domains may appear similar to topological areas where the Fermi level crosses the Dirac point. We have shown that the effects of topological domain disorder can be distinguished from other forms of disorder by considering the energy dependence of the pattern of the fluctuation of density of states (also known as quasiparticle interference). Another relevant issue regarding the LDOS measurement of the surface states using STM is the presence of large M pockets near the in-plane BZ corner at the same energy as the Dirac cone. Hence the states from the M pocket, in spite of them being from bulk bands, can contribute to the STM measured surface electronic density of states. However, states near the M pocket carry large momentum and the corresponding density oscillates at the scale of the in-plane lattice constant ($\simeq$0.4 nm), which is an order of magnitude smaller than the length scale of density fluctuations due to the proposed domain disorder ($\simeq$3 nm). Thus averaging of the electronic density over a length scale which is in between these two lengths should suppress the contribution from the states near the M pocket. As a relevant point we note that the experimental evidence of a nearly V-shaped density of states around the Dirac point [15], which is the characteristics of a 2D Dirac dispersion, indicates that the long wavelength surface state density is not affected by the states from any other nontopological bands.

As mentioned in the Introduction, our motivation to study the effect of alloy disorder on the topological surface states was based on its potential effect on the vortex MBSs. As an example of how local fluctuations in the topological character of a system can affect MBSs, consider a scenario where in

the SC state a vortex core penetrates through a trivial region on the top surface. Since the trivial region does not support topological states on the surface, such a vortex would not be expected to support any MBS. This would in principle be a potential explanation for the absence of MBSs in a large fraction of vortex cores in experiments [14,16]. Furthermore, such a topological domain disordered phase might also help explain the absence of quantized conductance in a large set of vortices [20]. This would occur when the trivial region is small in size relative to the superconducting coherence length so that the MBS wave function is still accessible to tunneling but at a reduced tunneling strength. Quantitative effect on the MBS wave function would depend on the actual correlation length for the alloy disorder and must be left to future work.

The alloy disorder that is natural in FTS can have other effects such as change in band width of the odd parity band and the topological gap. In fact, the disappearance of the topological surface state in experiments [24] can in principle arise from a reduction or shift in the topological gap as opposed to a change in the topological invariant discussed in the manuscript. However, since DFT calculations or experimental data are not available to estimate these effects, it is difficult to estimate at present. Furthermore, correlation between the alloy disorder, i.e., Te/Se positions, may complicate the analysis of the disorder effects. However, one can hope that these effects together with iron impurity induced Zeeman field [22] as well as nematic fluctuations and strain effects can be included into the surface state model to develop a complete understanding of the evolution of vortex level spectra with magnetic field [14].

ACKNOWLEDGMENTS

This work was supported by NSF QII-TAQS Grant No. 1936246. J.D.S. would also like to thank NSF Grant No. DMR-1555135 (CAREER) for support. We also thank J. Wang, J. Hoffman, P. Ghaemi, and R. Zhang for valuable discussions.

[1] Z. Wang, P. Zhang, G. Xu, L. K. Zeng, H. Miao, X. Xu, T. Qian, H. Weng, P. Richard, A. V. Fedorov, H. Ding, X. Dai, and Z. Fang, Phys. Rev. B **92**, 115119 (2015).
[2] G. Xu, B. Lian, P. Tang, X.-L. Qi, and S.-C. Zhang, Phys. Rev. Lett. **117**, 047001 (2016).
[3] H. Lohani, T. Hazra, A. Ribak, Y. Nitzav, H. Fu, B. Yan, M. Randeria, and A. Kanigel, Phys. Rev. B **101**, 245146 (2020).
[4] P. Zhang, K. Yaji, T. Hashimoto, Y. Ota, T. Kondo, K. Okazaki, Z. Wang, J. Wen, G. D. Gu, H. Ding, and S. Shin, Science **360**, 182 (2018).
[5] P. Zhang, Z. Wang, X. Wu, K. Yaji, Y. Ishida, Y. Kohama, G. Dai, Y. Sun, C. Bareille, K. Kuroda, T. Kondo, K. Okazaki, K. Kindo, X. Wang, C. Jin, J. Hu, R. Thomale, K. Sumida, S. Wu, K. Miyamoto *et al.*, Nat. Phys. **15**, 41 (2019).
[6] L. Fu and C. L. Kane, Phys. Rev. Lett. **100**, 096407 (2008).
[7] P. Hosur, P. Ghaemi, R. S. K. Mong, and A. Vishwanath, Phys. Rev. Lett. **107**, 097001 (2011).
[8] J.-P. Xu, M.-X. Wang, Z. L. Liu, J.-F. Ge, X. Yang, C. Liu, Z. A. Xu, D. Guan, C. L. Gao, D. Qian, Y. Liu, Q.-H. Wang, F.-C. Zhang, Q.-K. Xue, and J.-F. Jia, Phys. Rev. Lett. **114**, 017001 (2015).
[9] H.-H. Sun, K.-W. Zhang, L.-H. Hu, C. Li, G.-Y. Wang, H.-Y. Ma, Z.-A. Xu, C.-L. Gao, D.-D. Guan, Y.-Y. Li, C. Liu, D. Qian, Y. Zhou, L. Fu, S.-C. Li, F.-C. Zhang, and J.-F. Jia, Phys. Rev. Lett. **116**, 257003 (2016).
[10] Q. Liu, C. Chen, T. Zhang, R. Peng, Y.-J. Yan, C.-H.-P. Wen, X. Lou, Y.-L. Huang, J.-P. Tian, X.-L. Dong, G.-W. Wang, W.-C. Bao, Q.-H. Wang, Z.-P. Yin, Z.-X. Zhao, and D.-L. Feng, Phys. Rev. X **8**, 041056 (2018).
[11] A. Kitaev, Ann. Phys. (NY) **303**, (2003).
[12] C. Nayak, S. H. Simon, A. Stern, M. Freedman, and S. Das Sarma, Rev. Mod. Phys. **80**, 1083 (2008).
[13] M. Sato and Y. Ando, Rep. Prog. Phys. **80**, 076501 (2017).
[14] T. Machida, Y. Sun, S. Pyon, S. Takeda, Y. Kohsaka, T. Hanaguri, T. Sasagawa, and T. Tamegai, Nat. Mater. **18**, 811 (2019).
[15] D. Wang, L. Kong, P. Fan, H. Chen, S. Zhu, W. Liu, L. Cao, Y. Sun, S. Du, J. Schneeloch, R. Zhong, G. Gu, L. Fu, H. Ding, and H.-J. Gao, Science **362**, 333 (2018).
[16] X. Chen, M. Chen, W. Duan, X. Zhu, H. Yang, and H.-H. Wen, arXiv:1909.01686.
[17] L. Kong, S. Zhu, M. Papaj, H. Chen, L. Cao, H. Isobe, Y. Xing, W. Liu, D. Wang, P. Fan, Y. Sun, S. Du, J. Schneeloch, R. Zhong, G. Gu, L. Fu, H.-J. Gao, and H. Ding, Nat. Phys. **15**, 1181 (2019).
[18] C. Caroli, P. D. Gennes, and J. Matricon, Phys. Lett. **9**, 307 (1964).
[19] M. Chen, X. Chen, H. Yang, Z. Du, X. Zhu, E. Wang, and H.-H. Wen, Nat. Commun. **9**, 970 (2018).
[20] S. Zhu, L. Kong, L. Cao, H. Chen, M. Papaj, S. Du, Y. Xing, W. Liu, D. Wang, C. Shen *et al.*, Science **367**, 189 (2020).
[21] C.-K. Chiu, T. Machida, Y. Huang, T. Hanaguri, and F.-C. Zhang, Sci. Adv. **6**, 9 (2020).
[22] A. Ghazaryan, P. L. S. Lopes, P. Hosur, M. J. Gilbert, and P. Ghaemi, Phys. Rev. B **101**, 020504(R) (2020).
[23] X. Wu, S. B. Chung, C. Liu, and E.-A. Kim, Phys. Rev. Res. **3**, 013066 (2021).
[24] Y. Li, N. Zaki, V. O. Garlea, A. T. Savici, D. Fobes, Z. Xu, F. Camino, C. Petrovic, G. Gu, P. D. Johnson, J. M. Tranquada, and I. A. Zaliznyak, Nat. Mater. **20**, 1221 (2021).
[25] M. B. Hastings and T. A. Loring, Ann. Phys. (NY) **326**, 1699 (2011).
[26] B. Estienne, N. Regnault, and B. A. Bernevig, Phys. Rev. B **86**, 241104(R) (2012).
[27] Z. Wang, J. O. Rodriguez, L. Jiao, S. Howard, M. Graham, G. D. Gu, T. L. Hughes, D. K. Morr, and V. Madhavan, Science **367**, 104 (2020).
[28] B. A. Bernevig, T. L. Hughes, and S.-C. Zhang, Science **314**, 1757 (2006).
[29] L. Fu and C. L. Kane, Phys. Rev. B **76**, 045302 (2007).
[30] X. Wu, S. Qin, Y. Liang, H. Fan, and J. Hu, Phys. Rev. B **93**, 115129 (2016).